atmosphere

MDPI

Article

Grey Cast Iron Brake Discs Laser Cladded with Nickel-Tungsten Carbide—Friction, Wear and Airborne Wear Particle Emission

Senad Dizdar [1,2], Yezhe Lyu [1], Conny Lampa [2] and Ulf Olofsson [1,*]

[1] Department of Machine Design, KTH—The Royal Institute of Technology, 100 44 Stockholm, Sweden; dizdar@kth.se (S.D.); yezhe@kth.se (Y.L.)

[2] Höganäs AB, Surface & Joining Technologies, 263 83 Höganäs, Sweden; conny.lampa@hoganas.com

* Correspondence: ulfo@md.kth.se; Tel.: +46-8-790-6304

Received: 8 May 2020; Accepted: 9 June 2020; Published: 11 June 2020



Abstract: Airborne wear particle emission has been investigated in a pin-on-disc tribometer equipped with particle analysis equipment. The pins are cut out from commercial powder metallurgy automotive brake pads as with and without copper content. The discs are cut out from a commercial grey cast iron automotive brake disc as cut out and as in addition to a laser cladded with a powder mix of Ni-self fluxing alloy + 60% spheroidized fused tungsten carbide and then fine-ground. Dry sliding wear testing runs under a contact pressure of 0.6 MPa, sliding velocity of 2 m/s and a total sliding distance of 14,400 m. The test results show both wear and particle emission improvement by using laser cladded discs. The laser cladded discs in comparison to the reference grey cast iron discs do not alter pin wear substantially but achieves halved mass loss and quartered specific wear. Comparing in the same way, the friction coefficient increases from 0.5 to 0.6, and the particle number concentration decreases from over 100 to some 70 (1/cm^3) and the partition of particles below 7 µm is approximately halved.

Keywords: airborne particle emission; pin-on-disc; friction; wear; grey cast iron; laser cladding; tungsten carbides

1. Introduction

For many years grey cast iron (GCI) brake discs have been a state of art in the automotive industry offering a good braking performance for an affordable cost [1]. One the other hand, GCI has a low corrosion resistance when exposed to increased atmospheric humidity and road salt. Corrosion alone or in synergy with wear can both shorten the useful service life and lower the braking performance of GCI brake discs because of the oxide layers on the braking surfaces [2–4].

A problematical aspect in using GCI brakes is the generation of airborne wear particles—dust during vehicle braking cycles. This dust includes particulate matter in different sizes, which can be respired and cause serious health problems. Particles less than 2.5 micrometers in diameter, also known as fine particles or PM2.5, pose the greatest risk to health. The smaller particles mean the higher risk for their penetration into living organisms. Miguel et al. [5] reported that paved road dust from bypassing vehicles acts as a significant source of air pollution. This is noticeable in urban areas with poor vegetation and close to highways with dense traffic. Brake dust was pointed out by Harrison et al. [6] to participate for more than 50% in particle size from 0.9 to 11.5 µm at a few selected London's streets. These findings about harmfulness of paved road dust and brake dust promoted the research on airborne particle emissions from disc brake contact. Olofsson et al. developed a model pin-on-disc with airborne wear particle emission analysis instruments [7], simulating and ranking the brake pad to brake disc contacts regarding airborne particle emissions [8–12].

A way to reduce airborne wear particle emission appears to be coating and overlay welding of GCI brake discs. Two techniques have been in focus: high velocity oxy-fuel (HVOF) spraying and laser cladding (LC). Thin, about 0.3 mm in thickness, HVOF sprayed tungsten carbide-cobalt (WC-Co) or tungsten carbide-cobalt-chrome (WC-Co-Cr) have been investigated [9,10,13] and are already industrially applied in premium passenger car segment [14,15]. The coatings possess high density (over 98% of the theoretical pore-free density), high hardness and fine microstructure but limited adhesion strength to the base metal in the order of 60 MPa, see Fauchais et al. [12]. The relatively small pore content in the coating may allow corrosion agents to reach the base metal and drop the coating performance. Therefore, the coatings demand a fully dense buffer layer over the GCI surface. The WC-Co and WC-Co-Cr powder consumables sourcing can include high price fluctuation since W- and Co-mineral ores are with limited availability and can belong to conflict minerals [16]. The wear appears to be very low [15], but very small amounts of harmful PM10 and PM2.5 particles are still emitted into the environment. REACH regulation of the European Union, see Appendix A, classifies a large majority of industrial substances according to their assessed toxicity/harmfulness. Co as a substance has classified hazards and recognition/suspicion concerns on skin and respiratory sensitizing. However, the concerning includes some doubts, and there is no wide consensus on how toxic cobalt is. There is ongoing research and development on replacement of Co-matrix in WC-Co and WC-Co-Cr powder alloys for iron/stainless steel but so far with a limited extent see, e.g., [17]. For W- and WC-substances, the REACH classifications and concerns are much less serious.

Laser cladding [18–20] is of particular interest for overlay welding of the GCI brake disc. It offers metallic or metallic/ceramic weld overlays with metallurgical bonding to the base metal. It features small heat affected zone, low dilution of the base metal in the weld overlay and low thermal deformation of the weld blank [21]. In combination with stainless steel powder alloys as welding consumables [22], it opens for wear and corrosion resistant hard faces for GCI brake discs. Used brake discs can be repaired by laser cladding instead of being scraped and remelted with high energy consumption and unnecessary emission of CO_2. Fruehan et al. [23] report some theoretical/practical assessments of about 445 kWh/ton in energy respective to 280 kg/ton in CO_2 emission for steel production from steel scrap in an electric arc furnace. A rough estimation of energy consumption for laser cladding is about 130 kWh/ton (a brake disc of 13 kg cladded for 10 min with 10 kW total laser unit power). Gramstat et al. [20] reported about brake dynamometer testing of GCI brake discs overlay welded with hard metal- and metal-alloys including a stainless steel buffer overlay. The hard metal alloys are not specified in detail but according to cross sectional views of the overlays, it is likely to be deposited by laser cladding and using a powder mix of Ni-self fluxing base powder (Ni-SF) and over 50% spherical fused tungsten carbides (SFTC). The metal alloy is likely to be a non-stainless steel alloy. The friction and wear outcomes are both promising. The friction coefficient is quite constant at a level of 0.3 for both alloys, while the brake disc wear drops to 10% and 7% and the brake pad wear to 80% and 55% for hard metal respective metal overlays. However, the overlays include cracks and are to be further developed. Ni, is according to the REACH regulation, see Appendix A, a substance described in similar to Co. Ni as matrix material is known to offer virtually no solubility for C from carbides or the blank material during welding and this property is not easy to find at other metallic matrix alloy. There is ongoing research and development on for example stainless steel [19] as a potential Ni replacement.

Investigations [10–15,20] show that carbides in various form contributes to a reduction of wear and airborne wear particle emission. In particular, investigation [18] appears to need a completion to clarify friction, wear and airborne wear particle emission of Ni-SF/SFTC weld overlays. Relatively coarse and densely distributed SFTC particles will carry out the friction and wear loading and it may affect the airborne particle emission. So far, a stainless steel matrix for SFTC carbides is not available and the Ni-SF matrix can be used because the focus is on how the SFTC carbides affect the airborne particle emission. Therefore, the aim of this investigation is to generate reference data on friction, wear and wear particle emission for laser cladded Ni-base/SFTC overlays of GCI brake discs by using pin-on-disc testing and compare the results with previous reports.

2. Experiments

Table 1 lists manufacturing routes for the test discs and pins. GCI test discs were cut-out and machined from commercial automotive brake disc. Test pins were cut-out and machined from commercial low-metallic automotive brake pads.

Table 1. Test samples.

		Pin/Cu-Contained	Pin/Cu-Free	GCI	GCI/LC	
Dimension (mm)		**ø10 × 25**	**ø10 × 25**	**ø60 × 6**		
Test Surface—Test Cladded Surface	Manufacturing Process	Commercial brake pad	Commercial brake pad	Commercial brake disc		
		Water jet cutting	Water jet cutting	Water jet cutting		
		Turning	Turning	Turning		
				-	Laser cladding [1] with 1535-30 +60% 4590 powder mix (Höganäs AB) conforming to EN 14,700 P Ni20	
					Super-abrasive grinding [2]	
	Composition [3]	Low-Metallic Brake Pad	Low-Metallic Brake Pad	Grey Cast Iron (GCI)	Powder Mix, mass %. (Cladding Includes 5% Fe-Dilution),	
					1535-30	+60% 4590
	Al	10.7	8.8	0.5	1	0
	B	N/A	N/A	N/A	1	0
	Bi	1.6	0.8	0	0	0
	C	N/A	N/A	N/A	0.24	4
	Ca	2.4	1.6	0	0	0
	Cr	3.4	1.9	0.2	5.7	0
	Cu	15	0.1	0.2		0
	Fe	15	24.8	95.4	2.5	0
	Mn	0.2	0	0.6	1	0
	Ni	0.1	0.4	0.2	(86.66) bal.	0
	P	0.6	0	0	0	0
	S	0	11.1	0.2	0	0
	Si	0	6.6	1.8	2.9	0
	Sn	15.4	10.6	0	0	0
	Ti	0.4	11.9	0	0	0
	Zn	25	18.8	0	0	0
	W	0	96	0	96	(96) bal.
	Total	98.8	97.4	99.1	100	100
	(Others)	1.2	2.6	0.9	-	-
	Comment	Indication	Indication	Indication	Nominal	Nominal
	Hardness	N/A, indication 60–70 HRH		<20 HRC	58 HRC	
	Specific density g/cm^3	2.75	2.75	7.1	13.58	
	Roughness, 2D	As delivered		As turned	As ground (l_c = 0.8 mm)	
	R_a (µm)	10.2		1.76	0.08	
	R_z (µm)	101		12.7	0.95	
	R_{sk} ()	−0.28		−1.35 (! Biased *)	−1.58	
	R_{sm} (µm)	−720		210	354	
	Cut-off l_c (mm)	2.5		0.8	0.8	
	Comment	As indication only		* Several deep pores	Smooth.	

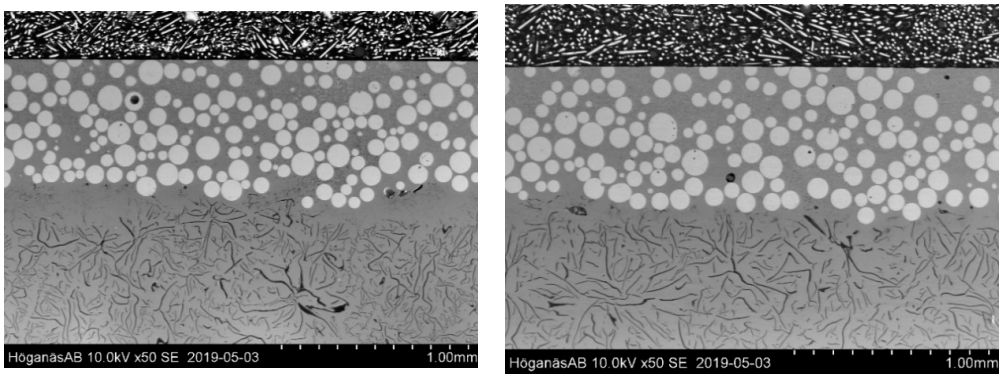
[1] Fiber coupled diode laser (Laserline LDF 7 400), powder nozzle (Three-jet, Fraunhofer ILT), ø2 mm laser spot, laser power 950 W, 50% overlap, laser head travel speed 8 mm/s and powder feed rate 7 g/min. Cladding thickness approx. 0.8 mm as ground. Overlay dilution 5% (Fe). [2] Vertical axis grinding machine (Göckel G50 elT); 6A2 shaped, 126-FEPA-grit diamond coated grinding wheel (Tyrolit Startec-Basic), cutting depth 0.005-0.01 mm (less than half of as commonly recommended cutting depth 0.025 mm), extreme-pressure (EP)-mineral oil based cutting fluid. [3] By using X-ray fluorescence (XRF)-gun analyzer (Thermo Scientific Niton XL3t GOLDD + XRF Analyzer), ø8 mm spot, 50 kV.

Cladded test discs were manufactured by laser cladding of a batch of present GCI discs. The laser cladding was performed by using a 7 kW fiber-coupled diode laser (Laserline LDF 7000-40). This laser had a high beam quality expressed as 44 mm·mrad. That allows the laser beam to be transported by a process fiber as small as 400 µm to the processing head. When reaching the target surface, it will have a quasi-uniform energy distribution within the circular laser spot. The metal powder was injected to the process zone by a coaxial powder nozzle (Three-jet, Fraunhofer ILT) that allows cladding with a stand-off distance of 16–17 mm and spot size of ø2 and ø5 mm. For the present discs, the following parameters were used: laser spot ø2 mm, laser power 950 W, weld bead overlaps 50%, laser head

travel speed 8 mm/s and powder feed rate 7 g/min. The parameters' combination was chosen in order to minimize the heat input into 6 mm thick disc substrate. Neither preheating nor annealing were performed on the test discs. The cladded discs were then super-abrasive ground. The as ground cladding surface reached 58 HRC in hardness and as expected 5% iron dilution evaluated by an XRF-hand held analyzer (Thermo Scientific Niton XL3t GOLDD+ XRF Analyzer), having ø8 mm spot and 50 kV energy range.

The metal powder consumable was 1535-30 + 60 mass % 4590 mix (by Höganäs AB), see Table 1. Base powder 1535-30 was a Ni-SF powder grade with low affinity to alloying with carbon and 4590 was an SFTC powder with a micro hardness of up to 2600 $HV_{0.1}$ and melting point exceeding 2500 °C. Both powders had a sieve cut of 53–150 µm. The powder mix flow rate was 8.5 s/50 g and Hall-apparent density is 6.8 g/cm^3.

Figure 1 shows cross sectional metallographic view of the laser cladded test discs in as ground partition. The SFTC carbides distribution is quite even and the carbides do not show any signs of a severe dissolution. The graphite from the GCI lamellas neither climb into the cladding nor contribute to the formation of gaseous voids.



(**a**) (**b**)

Figure 1. Cross sectional view of laser cladded test discs in as ground partition. (**a**) Test run with Cu-free pins and (**b**) test run with Cu-contained pins.

The wear testing and the resulting airborne wear particle emission acquisition were performed in a testing cell [7]. The cell consisted of a commercial pin-on-disc tribometer (VTT) in a sealed polycarbonate enclosure with an air handling system and particle emission analyzers, see Figure 2. The tribometer had a robust design. An AC motor rotated a test disc about its vertical axis. A load arm assembly with dead weights pressed a test pin in vertical position against the test disc. The tribometer could run at a normal load up to 120 N and rotational velocities 10–3000 rpm. A 200 N load cell (HBM® Z6FC3, max. non-linearity of 0.1% of the full-scale), i.e., records the friction force.

Mass loss of the test specimens was assessed by weighing the test samples before and after the test to the nearest 0.1 mg using a lab balance (Sartorius® ME614S). The specific wear rate k in mm^3/(N·m) for each specimen can then be determined as

$$k = \frac{\Delta m}{\rho \times \Delta s \times F_n}$$

where Δm is the mass loss of the specimen, ρ the specific density of the specimen, Δs the sliding distance during the test, and F_n the normal load applied on the pin. This method enables the calculations of the specific wear rate of the pin. For specific wear calculation of the test disc, some simplifications had to be made. The pin with diameter of ø10 mm slides against the disc on a radius of 25 mm. For one-disc revolution, a single point of the disc achieves a sliding distance equal to the pin diameter, i.e., 10 mm. For a total test sliding distance of 14,400 m and a sliding velocity of 2 m/s, the disc rotates 91,673 revolutions. In that way, a point on the test disc wear track would be exposed to a sliding distance of 916.7 m.

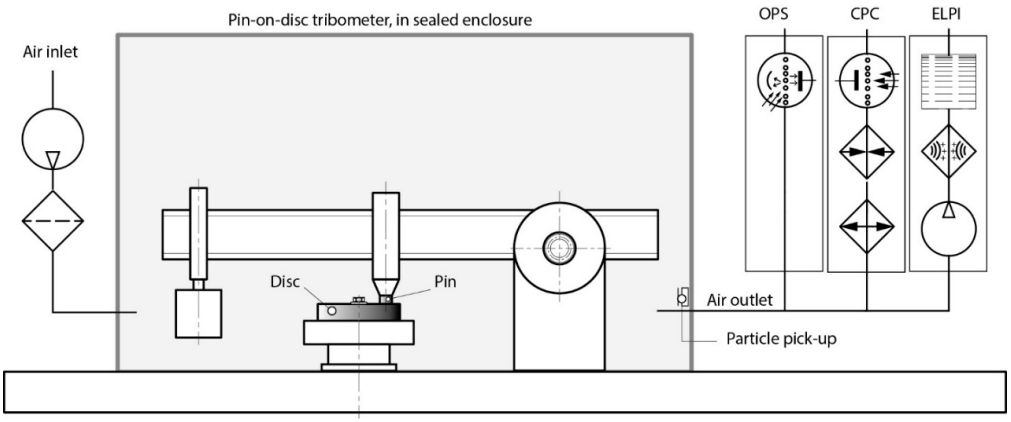


Figure 2. Schematic of the particle emission testing cell consisting of a pin-on-disc tribometer in a sealed enclosure. The room ambient air is pumped to the enclosure but first cleaned from particles by using a high efficiency particulate air (HEPA)-filter. Three particle emission analyzers are connected to the air outlet, an optical particle sizer (OPS), a condensation particle counter (CPC) and an electrical low-pressure impactor (ELPI).

To enable particle emission measurements, a sealed polycarbonate enclosure enclosed the tribometer (Figure 2). The air inlet assembly consisted of a fan that pumped in ambient air through a high efficiency particulate air (HEPA) filter. The HEPA filter is of class H13 according to EN 1822 norm with a declared collection efficiency of 99.95% at the maximum penetrating particle size. It ensures a virtually particle free inlet air. The inlet air velocity was measured with a TSI® air velocity transducer Model 8455. Due to the complex volume of the pin-on-disc tribometer and the high exchange rate, the air was well mixed. The volume of the air inside the box was about 0.1 m^3. The air flow in the box transported the generated particles to the air outlet, where a sampling point was located with hose inlets of three particle emission analyzers.

The main particle counting instrument in this study measured particle number concentration and size distribution in the size range of 0.3–10 µm in 16 user adjustable size channels (TSI® Optical Particle Sizer (OPS) model 3330). The sampling frequency was 1 Hz for the instrument.

The OPS is sensitive to the form and refractive index of the particles, which means that the measured particle sizes and number distributions should be regarded as approximate [24]. The OPS is calibrated with polystyrene latex spheres (PSL), which has a different size distribution, density and refractive index to the particles generated by disc brakes. The output from the particle instruments will only be used as relative measures, which are useful when ranking different material combinations with respect to particle emissions. The measures can also be used to show changes in the number concentration in real-time.

In addition, very close to the hose inlet hole, an aluminum button ø25 × 5 mm covered with double-adhesive carbon-conductive tape (Ted Pella prod No. 16073) was mounted inside the enclosure in order to collect and visualize the wear particles close to the inlet of the particle emission instruments.

The temperature and humidity inside the box were not controlled but they should not differ from the common laboratory room conditions, i.e., a temperature of 20 °C and a relative humidity of 50%.

3. Results

Achieved friction coefficient and wear of the test pins and discs are shown in Figures 3 and 4. To note, the friction coefficient shown are representative ones. The tests with GCI discs resulted in a steady state friction coefficient of about 0.5 disregarding the copper content of the test pins. The cladded discs, in contrast, show a steady state friction coefficient of 0.6 for copper containing pins and 0.65 for copper-free pins. Different components of the pad and disc material affects the coefficient of friction achieved in the contact between them. In this case a probably cause of the increase in the coefficient of friction when using the laser cladded material was the reduction of carbon in the surface layer.

This increase in the coefficient of friction is not, a problem for the use in a disc brake. The brake pressure as assigned by the driver can adapt the increase of the coefficient of friction.

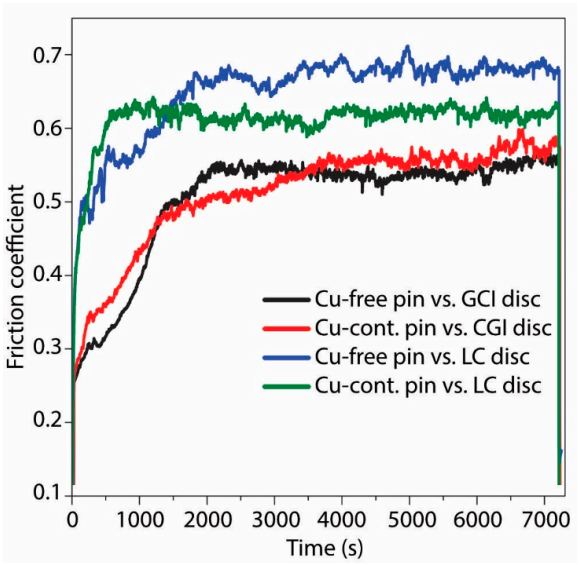


Figure 3. Time history of friction coefficient representative tests from four material combinations. Testing conditions are dry sliding wear at sliding velocity of 2 m/s, contact pressure 0.6 MPa for 2 h. The effective sliding distance is 14.4 km.

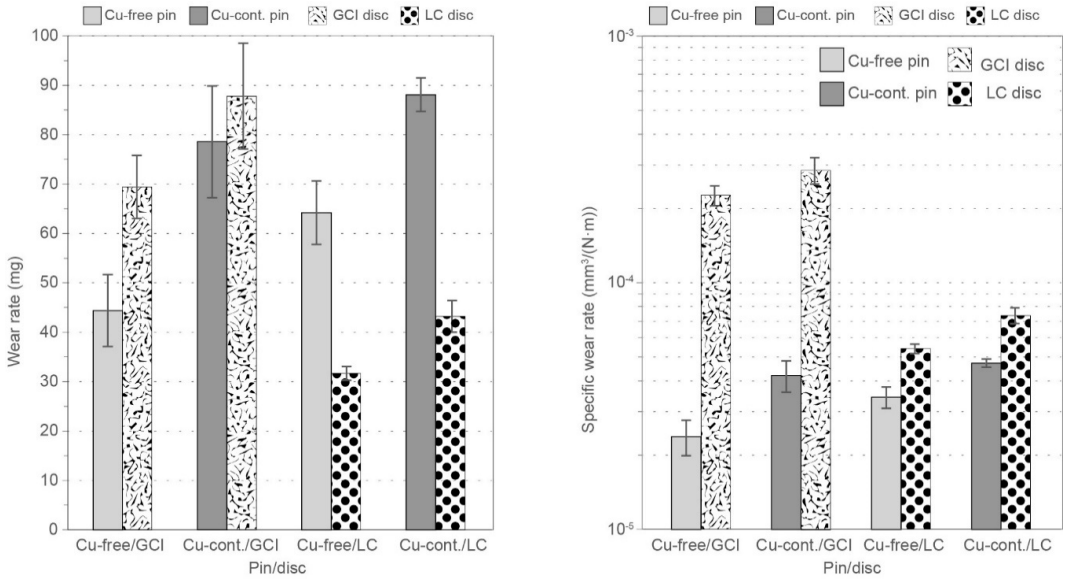


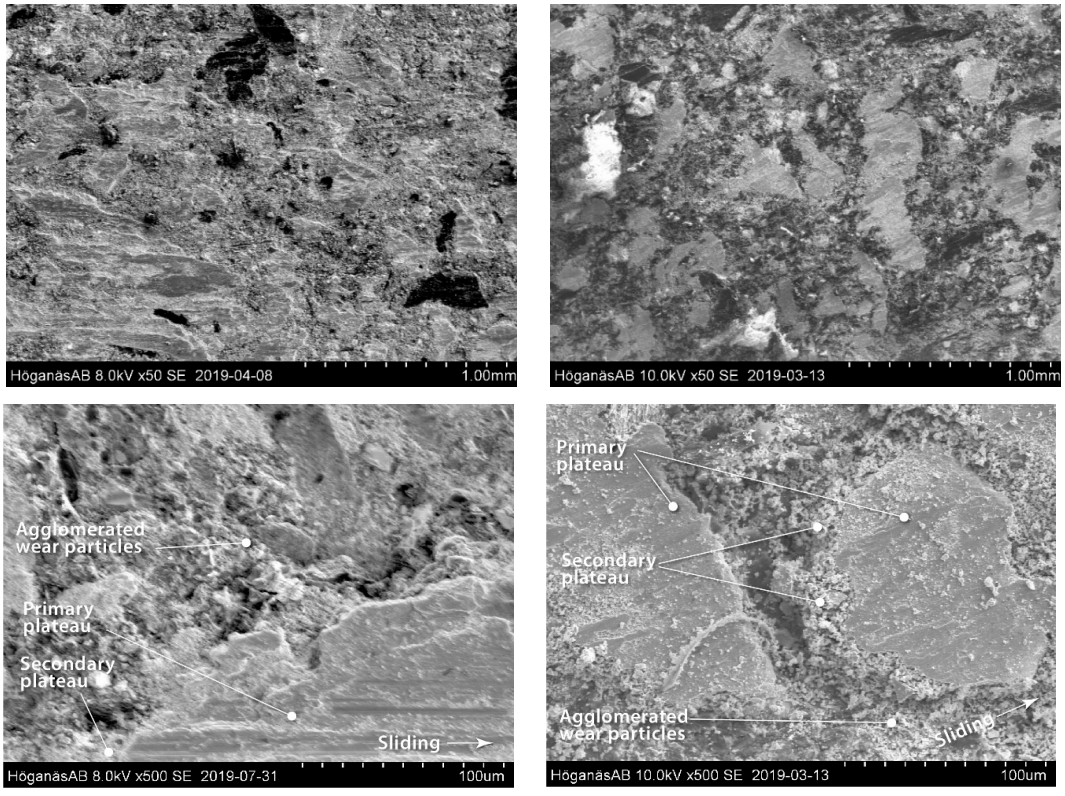
Figure 4. Pin wear and disc wear corresponding to the whole test duration. Testing conditions are dry sliding wear at sliding velocity of 2 m/s, contact pressure 0.6 MPa for 2 h. The effective pin sliding distance is 14.4 km.

Wear of the copper free pins was lower than that of the copper-containing pins disregarding the test discs. Wear of the pins mated with GCI discs was lower than that with laser cladded discs. The wear as mass loss was 44 and 79 mg for copper–free and copper contained pins mated with GCI discs and the corresponding specific wear rate was 2.4×10^{-5} and 4.2×10^{-5} mm^3/(N·m). Mass loss of the pins mated with LC discs was 64 and 88 g with corresponding specific wear rate 3.4×10^{-5} and 4.7×10^{-5} mm^3/(N·m) for copper–free and copper contained pins. The pin wear when mated with GCI discs agrees with results of Wahlström et al. [25]. As seen, the pin wear slightly increased for

laser cladded discs. The presence of the hard SFTC-phase and absence of graphite on the contact area comparing to the GCI discs might be listed as apparent reasons.

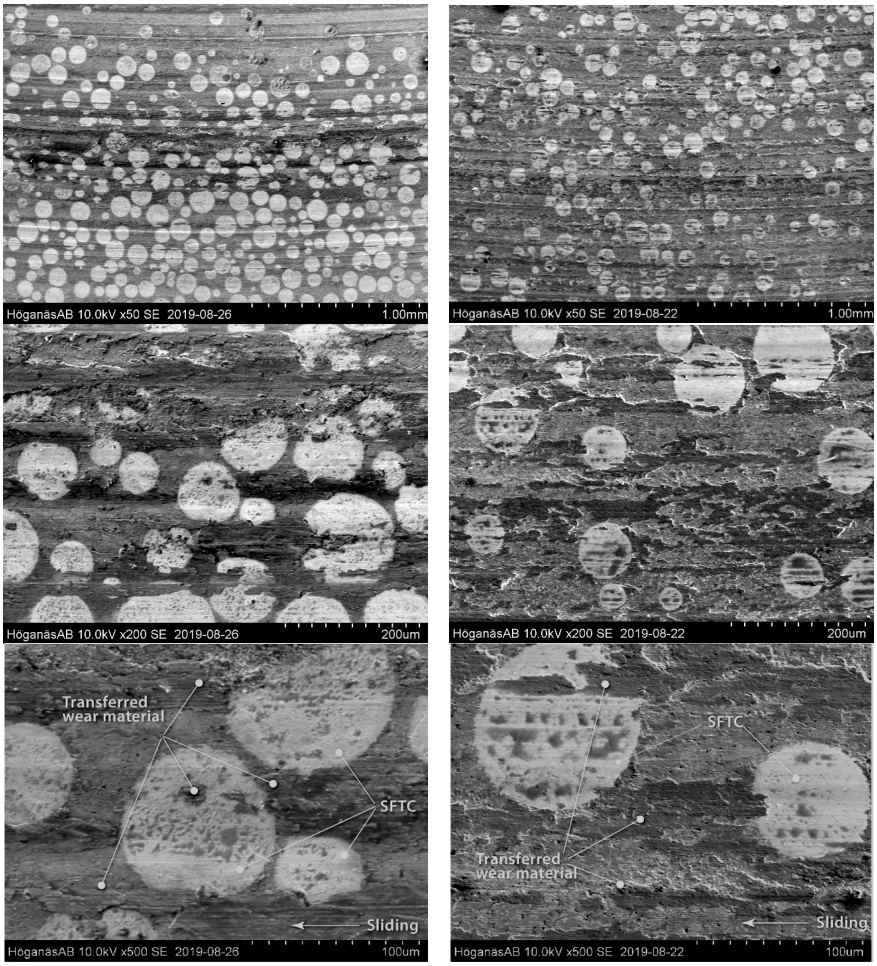
For disc wear, the picture was different. The laser cladded discs roughly achieved halved mass loss and quartered specific wear rate of the GCI discs for copper-free and copper contained pins. To note, it occurred under the higher friction coefficient, 0.6–0.65. Mass loss of GCI discs was 69 and 88 mg with corresponding specific wear rate 2.3×10^{-4} and 2.9×10^{-4} mm^3/(N·m). For laser cladded discs, the numbers were 32 and 43 mg as well as 5.4×10^{-5} and 7.4×10^{-5} mm^3/(N·m). Here it must be commented that an insignificant level of error could be present in specific wear calculation for laser cladded discs. The specific density of the cladding was not possible to evaluate with a high precision without a costly and resource demanding procedure. Here the cladding was assumed to include 40% NSF-matrix and 60% SFTC, the same mass percentage ratio as for the powder mix, and the calculated specific density was 13.6 g/cm^3. Assuming a reasonable deviation of the percentage ratio, 50% NSF-matrix and 50% SFTC, the density dropped to 12.8 g/cm^3, the specific wear rate decreased for 6%, but it changed neither the wear ranking nor significantly the absolute wear levels.

The friction and wear description were to be completed with the appearance of the worn pin and the laser cladded disc contact surfaces, see Figures 5 and 6. Both copper free- and copper–contained test pins show the formation of primary and secondary wear plateaus and wear particle agglomerates as it can be expected [26–28]. The plateaus show adhered wear particles of micrometer-level size. The test discs show wear tracks with both relatively shallow and wide scars due to plasticity-dominated wear as well as narrow and sharp scars due to abrasion. Material transfer is obvious, thin transferred layers cover both the Ni-SF-matrix and the SFTC. EDS mapping analysis on the transferred layers (Bruker Quantax EDS with XFlash 1050 detector, 15 kV) revealed strong signals for O, Ca, Zn, Al, S and Cr for disc from the run with Cu-free pins. In the Cu-contained pins, Cu is detected in addition. The presence of overlapped O and Al regions verified alumina, Al_2O_3, content, while the presence of S of the pins verified solid lubricant content in the pins.



(**a**) (**b**)

Figure 5. Detailed top views of pin wear track from runs with Cu-free (**a**) and Cu-contained pin (**b**).



(**a**) (**b**)

Figure 6. Top views of laser cladded disc wear tracks from runs with Cu-free (**a**), and Cu-contained pin (**b**) in magnifications 50, 200 and 500 times for top, mid respectively bottom row in order to get a more complete picture about the wear track.

Results of particle emission analysis are shown in Figures 7–9. From Figure 7, one sees roughly halved particle number concentration (PNC) for laser cladded test discs of 60 and 50 particle/cm^3 compared to those of GCI discs 150 and 120 particle/cm^3. This overall 50% reduction in PNC was in parallel to what was achieved by adding on particle filters for disc brake systems or changing to HVOF coated disc (WC-Co-Cr) where a reduction of particle emissions of 50% could be demonstrated [25]. In parallel, the friction coefficient rose up, from 0.53 and 0.53 for GCI test runs to 0.65 and 0.6 for laser cladded test discs. The time history of the PNC in Figure 8 shows no correspondences with the time history of the friction coefficient in Figure 3. It is interesting to note that the cu free as well as the cu containing pin emitted a similar level of PNC when sliding on laser cladded discs this in contrast to the standard CGI disc where the cu free pin emitted more particles than the cu containing one. Over the years, Cu has proved to be an important ingredient in brake pads and it improves the thermal conductivity of brake pads, helps to build up a compact friction layer and decrease the wear rate of brake pads [10]. In this study with a laser clad disc the results shows lower wear for the cu free pins and a similar level of airborne particle concentration.

Figure 9 shows particle size distribution in the steady state. The shapes of the distribution curves were similar except the size range below 0.7 µm. For a particle size below 0.7 µm, laser cladded disc test runs in comparison to GCI ones achieved lower particle number concentration. For particle size below 0.5 µm, this decrease was down to one half. Of note, the smaller the particles, the more deeply they will penetrate into the organs.

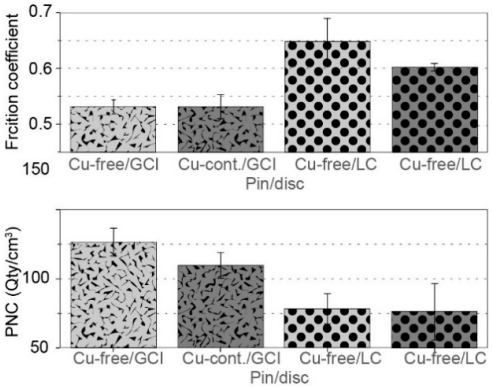


Figure 7. CoF (friction coefficient) and PNC (particle number concentration) in the steady state.

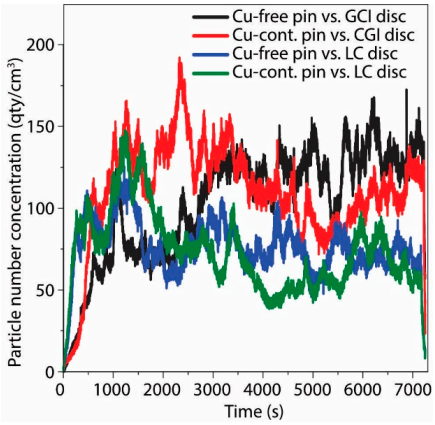


Figure 8. Time history of particle number concentration of representative tests from four material combinations.

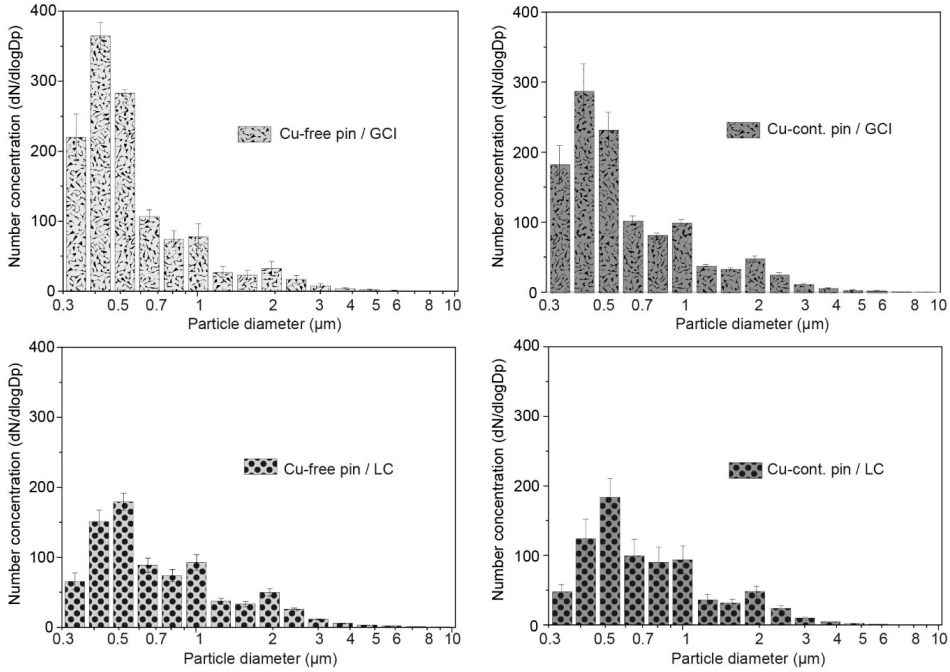
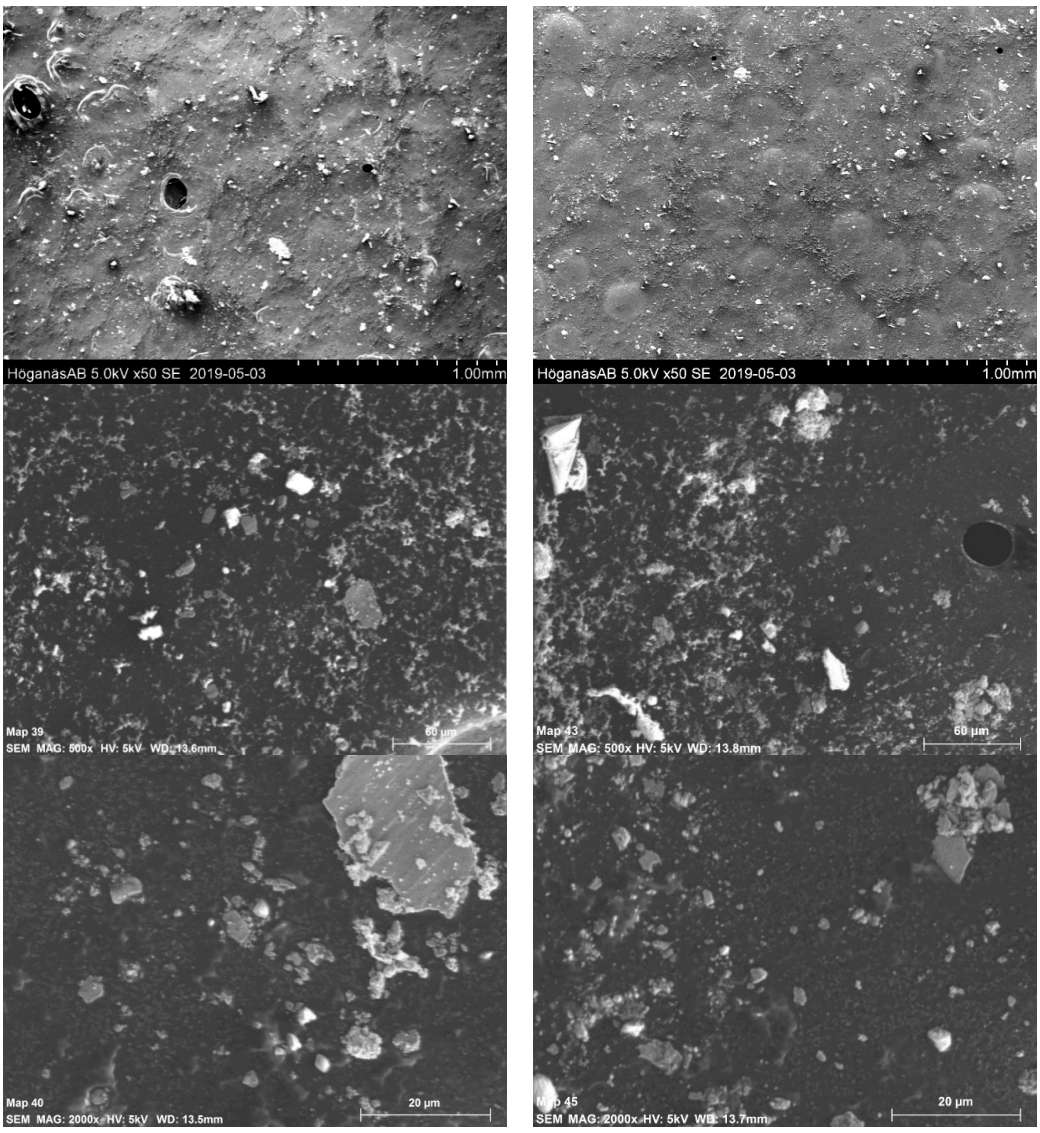


Figure 9. Particle size distribution in the steady state. For the cast iron disc test runs, the highest peak is the second bar (channel two in the optical particle sizer (OPS)) and for the laser cladded test runs, the highest peak is the third bar (channel three in OPS).

Figure 10 shows wear particles trapped onto ø25 mm aluminum buttons covered with double-adhesive carbon tape in runs with Cu-free and Cu-contained pins mated LC discs. The buttons were quite evenly covered by the wear particles as seen at 50× magnification. Large magnifications, 500× and 2000×, gave insight in the size and form of the particles. A large range of particle size was seen. The largest particles appeared to be over 20 µm and the smallest ones far below 1 µm. These particles look like as crushed parts of the plateaus shown in Figure 5. The form for relatively larger particles appeared to vary from angular to subangular in roundness and from low to mean sphericity following the Power's roundness–sphericity chart of sedimentary particles [26]. Some of the particles appeared like a cluster of crushed particles. A similar particle morphology has been identified by Nosko et al. [29]. Very few particles, i.e., chip-like being thin and long, with low sphericity were found. The trapped particles as shown appeared to be crushed during wear and/or inheriting their formation during solidification or sintering process. This contrasts with smeared transferred material on the wear track of the laser cladded test discs (Figure 6).



(**a**) (**b**)

Figure 10. Wear particles trapped onto ø25 × 5 mm aluminum buttons covered with double-adhesive carbon tape. The button placing is just over the outlet hole of the tribometer enclosure. Photos are in magnification of 50, 500 and 2000 times for top, mid respectively bottom row in order to get a complete picture of distribution and size of the wear particles. (**a**) Cu-free pin and (**b**) Cu-contained pin.

Load-bearing contact area of the laser cladded test discs is to the largest extent provided by the SFTC-phase in the overlay microstructure. This is for sure an important reason for lower wear and wear particle emission of the laser cladded discs. A principal change in the metal matrix alloy, from the Ni-SF-based one to the Fe-based one should not change much in the load bearing area of the laser cladded test discs [30]. Therefore, the achieved reduction in wear and wear particle emission will likely be same for the Fe-based matrix base alloy.

4. Conclusions

Friction, wear and airborne wear particle emission were investigated in pin-on-disc tribometer equipped with particle analysis equipment. The pins were cut out from commercial copper free and copper contained powder metallurgy automotive brake pads. The discs were cut out from a commercial grey cast iron automotive brake disc as cut out and as in addition laser cladded with a powder mix of Ni-self fluxing alloy + 60% spheroidized fused tungsten carbide and then fine-ground. The laser cladding overlays achieved surface pattern of relatively coarse, 53–150 μm, and densely distributed SFTC-particles. Dry sliding wear testing runs under contact pressure of 0.6 MPa, sliding velocity of 2 m/s and a total sliding distance of 14,400 m. The following conclusions were drawn:

- Both wear and particle emission were reduced by using laser cladded discs compared to grey cast iron discs.
- The laser cladded discs in comparison to the reference grey cast iron discs:
    - Achieved halved mass loss wear and quartered specific wear without substantial increase in the pin wear.
    - The friction coefficient increased from the 0.5 level to the 0.6 level.
    - The particle emission concentration decreased about 30%, from over 100 to 70 particles/cm^3.
    - The size partition of particles below 7 μm was approximately halved.

Author Contributions: S.D. wrote the original manuscript draft, evaluated the tested surfaces and collected particles. Y.L. performed the tribological and aerosol measurements and analyzed this data. C.L. performed the laser cladding on the tested disc brake surfaces. U.O. together with S.D. formulated the research question and supervised the experiments. All authors contributed to the editing of the manuscript. All authors have read and agreed to the published version of the manuscript.

Funding: This research received no external funding.

Acknowledgments: The authors acknowledge the support of materials for testing provided by Mattia Alemani, Brembo, S.p.A.

Conflicts of Interest: The authors declare no conflict of interest.

Appendix A

The toxicity can be assessed by referring to the REACH regulation. REACH is accessible by using the European Chemical Agency (ECHA) website [31], where an introduction paragraph states that 'REACH is a regulation of the European Union, adopted to improve the protection of human health and the environment from the risks that can be posed by chemicals, while enhancing the competitiveness of the EU chemicals industry. It also promotes alternative methods for the hazard assessment of substances in order to reduce the number of tests on animals'. By compiling industrial participants' registered information on use, identified hazards and risks of substances, REACH opens for a safe use of the substances. Table A1 (See Appendix A) lists hazard classification and labeling as well as properties of concern for iron (Fe), carbon (C), chromium (Cr), nickel (Ni), cobalt (Co), manganese (Mn), tungsten (W), tungsten carbide (WC), silicon (Si) and quartz (SiO_2). The form in which the substances are considered varies, airborne wear particles PM10, PM2.5 and others are for sure included when considering skin and respiratory sensitizing, as well as allergies.

These substances are closely related to brake materials and braking events and are to be discussed. GCI and steels/stainless steels are the default respective potential material for brake discs but also the most important and most widely used technical materials. GCI includes mainly Fe, C (graphite) and Si as the constituents. Stainless steels alloys include Fe, C and corrosion resistance bearing substances such as Ni, Cr and Mo. Mn is often included in Fe-based materials as an alloying element in small or large contents. Cemented carbides such as WC-Co-Cr, WC-Ni-Cr or NiCr-CrxCy are important materials for wear protection by thermal spraying. Ni and Co work well as metal matrix substances but their suspected harmfulness opens for Fe as a desirable replacement. Fe-alloys cannot so far match Ni- and Co-alloy's performances in all the aspects. Metal matrix composites (MMC) to be weld overlaid are also important materials for wear protection. Ni-alloys are often used as the base material because of their exceptionally low affinity to carbon what is necessary to include carbides in the weld overlays. As for cemented carbides, Ni-alloy harmfulness opens for Fe-alloys as the matrix material, but so far Fe-alloy performances are still inferior to those of Ni-alloys. Quartz or silica is a material often present in brake pads but also added to braking systems from the asphalt or concrete road pavement or from the off-road areas.

Table A1. Brief description of metal powder and weld overlay included substances registered under European Union Regulation on Registration, Evaluation, Authorization and restriction of Chemicals (REACH), as found on web site of European Chemical Agency—ECHA [31]. The description is based on the so called "brief profile".

Substance, EC/List No. CAS No	Molecular Formula	Harmonized Hazard Classification and Labeling	Properties of Concern
Iron 231-096-4 7439-89-6	Fe	Classified Notified toxic to aquatic life, eye and skin irritation	(No)
Carbon (Graphite) 231-955-3 7782-42-5	C	No classified hazards Notified, eye and respiratory irritation	(No)
Chromium 231-157-5 7440-47-3	Cr	No classified hazards Notified, allergies and respiratory irritations	(No)
Nickel 231-111-4 7440-02-0	Ni	Classified Notified	C Officially suspected, C* (* Doubts) Ss Officially recognized, Ss* (* Doubts) Sr* (* Doubts)
Cobalt 231-158-0 7440-48-4	Co	Classified, aquatic life, allergies and respiratory irritations Notified	C* (* Doubts) Ss Officially recognized, Ss* (* Doubts) Sr* Officially recognized Sr* (* Doubts)
Molybdenum 231-107-2 7439-98-7	Mo	No classified hazards Notified, suspected of damaging fertility or the unborn child	(No)
Manganese 231-105-1 7439-96-5	Mn	Classified, aquatic life Notified	(No)

Table A1. *Cont.*

Substance, EC/List No. CAS No	Molecular Formula	Harmonized Hazard Classification and Labeling	Properties of Concern
Tungsten 231-143-9 7440-33-7	W	Classified / Notified	(No)
Tungsten carbide 235-123-0	WC	No classified hazards / Notified	(No)
Silicon 231-130-8 7440-21-3	Si	No classified hazards / No notified hazards	(No)
Quartz 238-878-4 14808-60-7	SiO_2	Classified, long/repeated exposure / No notified hazards	(** No overall agreement)

Key for Globally Harmonized System (GHS) pictograms [31] and labels; serious health hazard, health hazard, flammable, oxidizing, acute toxicity, hazardous to the environment; skin sensitizing, respiratory sensitizing and carcinogenic; (* inside pictogram) doubts that the property may relate to an impurity/additive rather than the substance itself. ** A minority of the industrial participants indicates the property.

Table A1 highlights in the harmonized hazard classification and labeling column that the majority of the substances have no GHS pictograms [32] for classified serious health hazard while Mo and Mn have notified serious health hazard. The minority of the substances with classification for serious health hazard includes Ni, Co and quartz. In a similar way, in properties of the concern column, majority of the substances are with no properties of concern. The minority with properties of concern includes again Ni, Co and quartz. Ni has official recognition for skin sensitizing and official suspect for carcinogenicity. Co has official recognition for skin and respiratory sensitizing. Then at the same time, there are doubts that these properties may relate to an impurity or additive rather than Ni respective Co itself. Quartz's property of concern is carcinogenicity but a minority of input registrations from the industry indicate it.

References

1. Maluf, O.; Angeloni, M.; Milan, M.T.; Spinelli, D.; Filho, W.W.B. Development of materials for automotive disc brakes. *Minerva* **2007**, *4*, 149–158.
2. Abdul Hamid, M.K.; Kaulan, A.M.; Syahrullai, S.; Abu Bakar, A.R. Frictional characteristic under corroded disc brakes. *Procedia Eng.* **2013**, *68*, 668–673. [CrossRef]
3. Djafri, M.; Bouchetara, M.; Busch, C.; Weber, S. Effects of humidity and corrosion on the tribological behaviour of the brake disc materials. *Wear* **2014**, *321*, 8–15. [CrossRef]
4. Noh, H.J.; Jang, H. Friction instability induced by iron and iron oxides on friction material surface. *Wear* **2018**, *400*, 93–99. [CrossRef]
5. Miguel, A.G.; Cass, G.R.; Glovsky, M.M.; Weiss, J. Allergens in Paved Road Dust and Airborne Particles. *Environ. Sci. Technol.* **1999**, *33*, 4159–4168. [CrossRef]
6. Harrison, R.M.; Jones, A.M.; Gietl, J.; Yin, J.; Green, D.C. Estimation of the contributions of brake dust, tire wear, and resuspension to non-exhaust traffic particles derived from atmospheric measurements. *Environ. Sci. Technol.* **2012**, *46*, 6523–6529. [CrossRef]
7. Olofsson, U.; Olander, L.; Jansson, A. A study of airborne wear particles generated from a sliding contact. *ASME J. Trib.* **2009**, *131*, 044503. [CrossRef]

8. Olofsson, U.; Olander, L. On the Identification of Wear Modes and Transitions Using Airborne Wear Particles Generated from Sliding Steel-on-Steel Contact. *Trib. Int.* **2013**, *59*, 104–113. [CrossRef]
9. Lyu, Y.; Leonardi, M.; Wahlström, J.; Gialanella, S.; Olofsson, U. Friction, wear and airborne particle emission from Cu-free brake materials. *Trib. Int.* **2020**, *141*, 105959. [CrossRef]
10. Alemani, M.; Wahlström, J.; Olofsson, U. On the influence of car brake system parameters on particulate matter emissions. *Wear* **2018**, *396*, 67–74. [CrossRef]
11. Abbasi, S.; Jansson, A.; Olander, L.; Olofsson, U.; Sellgren, U. A pin-on-disc study of the rate of airborne wear particle emissions from railway braking materials. *Wear* **2012**, *284*, 18–29. [CrossRef]
12. Fauchais, P.L.; Heberlein, J.V.R.; Boulos, M. *Thermal Spray Fundamentals—From Powder to Part*; Springer: Berlin, Germany, 2014.
13. Demir, A.; Samur, R.; Kilicaslan, I. Investigation of the coatings applied onto brake discs on disc-brake pad pair. *Metalurgija* **2009**, *48*, 161–166.
14. *Gusseisenbremsscheibe Gewinnt Deutschen Innovationspreis—Fachartikel*; DVS Media GmbH: Düsseldorf, Germany, 2018; Volume 9. (In German)
15. Elbrigmann, T. Hard like Diamond. *Porsche Cust. Mag. Christophorus* **2017**, *4*, 384.
16. Wikipedia. Available online: https://en.wikipedia.org/wiki/Conflict_resource (accessed on 4 May 2020).
17. Vilhena, L.M.; Fernandes, C.M.; Soares, E.; Sacramento, J.; Senos, A.M.R.; Ramalho, A. Abrasive wear resistance of WC–Co and WC–AISI 304 composites by ball-cratering method. *Wear* **2016**, *346*, 99–107. [CrossRef]
18. Toyserkani, E.; Khajepour, A.; Corbin, S. *Laser Cladding*; CRC Press: Boca Raton, FL, USA, 2005.
19. Zhang, Z.; Kovacevic, R. Laser cladding of iron-based erosion resistant metal matrix composites. *J. Manuf. Process.* **2019**, *38*, 63–75. [CrossRef]
20. Gramstat, S.; Wanninger, R.; Reinhold, B.; Sieber, H.; Eggenschwiler, P.D. Hard-metal coated brake discs—investigation of tribology, mechanical robustness and wear products, EB2019-MDS-020. In Proceedings of the Eurobrakes 2019, Dresden, Germany, 21–23 May 2019.
21. Davis, J.R. (Ed.) *Surface Engineering for Corrosion and Wear Resistance*; ASM Int.: Materials Park, OH, USA, 2001.
22. EN 14700, Welding consumables—Welding consumables for hard facing. In Proceedings of the European Committee for Standardization—CEN, Brussels, Belgium, 30 April 2014.
23. Fruehan, R.J.; Fortini, O.; Paxton, H.W.; Brindle, R. *Theoretical Minimum Energies to Produce Steel for Selected Conditions*; Carnegie Mellon University: Pittsburgh, PA, USA, 2000.
24. Grigoratos, T.; Martini, G. Brake wear particle emissions: A review. *Environ. Sci. Pollut. Res.* **2015**, *22*, 2491–2504. [CrossRef]
25. Wahlström, J.; Söderberg, A.; Olander, L.; Olofsson, U.; Jansson, A. A pin-on-disc simulation of airborne wear particles from disc brakes. *Wear* **2010**, *268*, 763–769. [CrossRef]
26. Powers, M.C. A new roundness scale for sedimentary particles. *J. Sediment. Petrol.* **1953**, *23*, 117–119. [CrossRef]
27. Wahlström, J.; Matjeka, V.; Lyu, Y.; Söderberg, A. Contact pressure and sliding velocity maps of the friction, wear and emission from a low-metallic/cast iron disc brake contact pair. *Trib. Ind.* **2017**, *39*, 460–470. [CrossRef]
28. Eriksson, M.; Bergman, F.; Jacobson, S. Surface characterization of brake pads after running under silent and squealing conditions. *Wear* **1999**, *232*, 163–167. [CrossRef]
29. Nosko, O.; Borrajo-Pelaez, R.; Hedström, P.; Olofsson, U. Porosity and shape of airborne wear microparticles generated by sliding contact between a low-metallic friction material and a cast iron. *J. Aerosol. Sci.* **2017**, *113*, 130–140. [CrossRef]
30. Wahlström, J.; Lyu, Y.; Matjeka, V.; Söderberg, A. Pin-on-disc tribometer study of disc brake contact pairs with respect to wear and airborne particle emissions. *Wear* **2017**, *384*, 124–130.
31. ECHA—European Chemical Agency. Available online: https://echa.europa.eu/ (accessed on 4 May 2020).
32. *Globally Harmonized System of Classification and Labelling of Chemicals*, 2nd revised ed.; United Nations: New York, NY, USA; Geneva, Switzerland, 2007; ISBN 978-92-1-116957-7.



© 2020 by the authors. Licensee MDPI, Basel, Switzerland. This article is an open access article distributed under the terms and conditions of the Creative Commons Attribution (CC BY) license (http://creativecommons.org/licenses/by/4.0/).